Structural Eng./Earthquake Eng. Vol. 10, No. 2, 83s—93s, July 1993
Japan Society of Civil Engineers (J. Struct. Mech. Earthquake Eng. No. 471/I—24)

IMPEDANCE FOR RIGID SQUARE FOUNDATION ON LAYERED MEDIUM

Gin-Show LIOU*

Presented are inpedance matrices for rigid square foundation on layered media and some numerical aspects for generating these impedance matrices. The analysis method employed is analytically solving wave equations in cylindrical coordinates, and then coordinate transformation, variational principle and reciprocal theorem are used to generate the impedance matrix for structural foundation. Since the interaction stresses between foundation and surrounding soil are assumed to be piecewise constant, the element size for the piecewise constant stress distribution is investigated. In order to demonstrate the reasonability of the assumed element size, some typical distributions of interaction stresses are presented. An example of a rigid square foundation rigidly attached to a two-layer medium and subjected to torsional, vertical, rocking and horizontal excitations is used to show the influence of layered stratum to the impedances.

Key Words : *impedance matrix, square foundation, layered medium*

1. INTRODUCTION

Due to the construction of heavy and stiff structures in the seismic areas in past few decades, the influence of seismic wave scattering on the structures attracts much attention. To deal with this soil-structure interaction problem, substructuring technique is normally employed. In the application of substructuring technique, the surrounding soil of structural foundation is represented by an impedance matrix, which can then be combined into total stiffness matrix of finite element model of structure for soil-structure interaction analysis. Therefore, to effectively and efficiently generate impedance matrix is an important step for the soil-structure interaction analysis.

There are procedures available for generating the impedance matrix; for examples : hybrid modelling[4),5)], boundary element method[6)~8)] and analytical approach[1)~3),9),10)]. In the hybrid modelling, the semi-infinite soil medium is divided into a far-field and a near-field. The far-field is modelled by either analytic or semi-analytic methods, and the near-field is modelled by standard finite element method. The conditions of stress and displacement continuities are then invoked at the interface of near-field and far-field. In the boundary element method, Green's function is employed as fundamental solution and reciprocal theorem is then used to minimize the error caused by the discrepancy between Green's function and finite element solution of structural foundation. In the analytical approach, the general solution of the differential wave equations for soil medium is used, and some numerical techniques are employed to obtain impedance matrix for soil-structure interaction analysis.

To obtain impedance matrix, no matter what procedure is employed, some discretization at the interface of foundation and soil is necessary. The accuracy of the impedance matrix and efficiency of computation are largely dependent upon discretization scheme of the interaction stresses. Therefore, the discretization scheme should be, as possible, in accordance with the distribution shape of the interaction stresses between foundation and surrounding soil. In other words, the element size at the contact region with sharp variation of interaction stresses should be small.

In the paper, a rigid square foundation rigidly attached to a two-layer medium and subjected to torsional, vertical, rocking and horizontal excitations is used as an example to study the impedance matrices, distribution of contact stresses, and their numerical scheme.

The analytical approach reported in References 1), 2), 3) is employed in the study. In the method, the general solution of three dimensional wave equations in cylindrical coordinates is employed for soil medium, and the contact stresses (interaction stresses) is assumed to be piecewise constant in rectangular coordinates. This assumed contact stresses are transformed into cylindrical coordinates. A special technique is then developed to decompose the transformed contact stresses in order to automatically match with the general solution of wave equations. After this, variational principle and reciprocal theorem are used to generate impedance matrix and interaction stresses.

Therefore, how to discretize the contact stresses

* Department of Civil Engineering, National Chiao-Tung University (Hsin-Chu, Taiwan 30049)

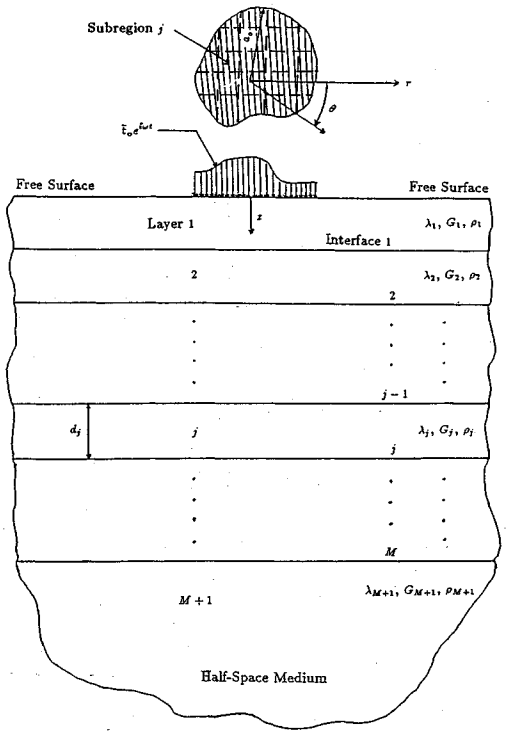

Fig.1 Dynamic Loading on Layered Medium

is an important factor for accurate and efficient computation in generating impedance matrix and distributions of the contact stresses. A discretization scheme by changing the size of constant contact stress elements is designed to investigate the accuracy of impedance matrix. Also, some typical contact stress distributions for torsional, vertical, rocking and horizontal motions of the square foundation are presented in order to show the reasonability of the discretization scheme. Some numerical results of the impedance matrices for different combinations of soil properties of the two-layer system are presented in order to show the effect of the layered stratum on impedance matrix.

2. STATEMENT OF ANALYSIS METHOD

The general solution of wave equations in cylindrical coordinates can be found by separating dilatational waves from rotational waves and using the technique of separation of variables[11]. To satisfy the boundary conditions due to existence of foundation, References 1), 2), 3) proposed a technique to decompose the boundary conditions in order to automatically match with the general solution. Then, by employing variational principle and reciprocal theorem and combining with finite element model of foundation structure, the distributions of interaction stresses between foundation and soil and the impedance matrix for the foundation are obtained.

A layered medium with precribed tractions having harmonic time history ($e^{i\omega t}$) at surface z=0 is shown in **Fig. 1**. The contact area can be divided into several subregions. In each subregion, the prescribed tractions are assumed to be constant.

$$\bar{t}_e^{\,i\omega t}=\begin{Bmatrix}\bar{\tau}_{xz}(x,y)\\ \bar{\sigma}_{zz}(x,y)\\ \bar{\tau}_{yz}(x,y)\end{Bmatrix}e^{i\omega t}=\sum_{j=1}^{m}\begin{Bmatrix}h_j(x,y)q_j\\ h_j(x,y)p_j\\ h_j(x,y)s_j\end{Bmatrix}e^{i\omega t}$$

$$=\begin{Bmatrix}\boldsymbol{h}^T\boldsymbol{q}\\ \boldsymbol{h}^T\boldsymbol{p}\\ \boldsymbol{h}^T\boldsymbol{s}\end{Bmatrix}e^{i\omega t}=\boldsymbol{HP}e^{i\omega t}\cdots\cdots(1)$$

where

$$h_j(x,y)=\begin{cases}1, & \text{if point } (x,y) \text{ in subregion } j\\ 0, & \text{otherwise}\end{cases}$$

m is the total number of the subregions, $3\times 3m$ matrix $\boldsymbol{H}=diag(\boldsymbol{h}^T,\boldsymbol{h}^T,\boldsymbol{h}^T)$, vector $\boldsymbol{P}^T=(\boldsymbol{q}^T,\boldsymbol{p}^T,\boldsymbol{s}^T)$, and q_j, p_j and s_j are the stress intensities in the subregion j for $\bar{\tau}_{xz}$, $\bar{\sigma}_{zz}$ and $\bar{\tau}_{yz}$ respectively. (The time harmonic variation $e^{i\omega t}$ will be omitted thereafter.)

Since the general solution of wave equations can be found in cylindrical coordinates, the prescribed tractions in Eq. (1) are transformed into cylindrical coordinates and then expressed in terms of Fourier components with respect to θ as follows :

$$\bar{t}_c=\begin{Bmatrix}\bar{\tau}_{rz}(r,\theta)\\ \bar{\sigma}_{zz}(r,\theta)\\ \bar{\tau}_{\theta z}(r,\theta)\end{Bmatrix}=\boldsymbol{T}\begin{Bmatrix}\bar{\tau}_{rz}\\ \bar{\sigma}_{zz}\\ \bar{\tau}_{yz}\end{Bmatrix}=\boldsymbol{THP}$$

$$=\sum_{n=0}^{\infty}(\boldsymbol{T}_n^s\bar{t}_n^s+\boldsymbol{T}_n^a\bar{t}_n^a),\quad 0\le r\le a_0\cdots\cdots(2)$$

where $\boldsymbol{T}$ is the coordinate transformation matrix and can be expressed as

$$\boldsymbol{T}=\begin{bmatrix}\cos\theta & 0 & \sin\theta\\ 0 & 1 & 0\\ -\sin\theta & 0 & \cos\theta\end{bmatrix}$$

a_0 is the distance from the origin to the farthest point on the contact area, matrix $\boldsymbol{T}_n^s=\text{diag}(\cos n\theta, \cos n\theta, -\sin n\theta)$, matrix $\boldsymbol{T}_n^a=\text{diag}(\sin n\theta, \sin n\theta, \cos n\theta)$, and superscripts s and a denote the symmetric and anti-symmetric components with respect to $\theta=0$ axis respectively. Applying the orthogonal property of Fourier series to Eq. (2) gives

$$\bar{t}_n^s=\begin{Bmatrix}\bar{\tau}^s{}_{rz,n}(r)\\ \bar{\sigma}^s{}_{zz,n}(r)\\ \bar{\tau}^s{}_{\theta z,n}(r)\end{Bmatrix}=\int_0^{2\pi}\boldsymbol{T}_n^s\boldsymbol{THd\theta P}\frac{1}{a_n}$$

and

$$\bar{t}_n^a=\begin{Bmatrix}\bar{\tau}^a{}_{rz,n}(r)\\ \bar{\sigma}^a{}_{zz,n}(r)\\ \bar{\tau}^a{}_{\theta z,n}(r)\end{Bmatrix}=\int_0^{2\pi}\boldsymbol{T}_n^a\boldsymbol{T}\boldsymbol{H}d\theta\boldsymbol{P}\frac{1}{a_n}\cdots(3)$$

where

$$a_n=\begin{cases}2\pi, & \text{if } n=0\\ \pi, & \text{if } n=1,2,\ldots,\infty\end{cases}$$

To solve three dimensional wave equations satisfying the boundary conditions of Eq. (2), principle of superposition can be applied. Therefore, one only needs to consider the boundary condition having one component $\boldsymbol{T}_n\bar{t}_n$ (either $\boldsymbol{T}_n^s\bar{t}_n^s$ or $\boldsymbol{T}_n^a\bar{t}_n^s$) of Eq. (2) in the solving process. Furthermore, the n^{th} Fourier component $\bar{t}_n$ of Eq. (2) can be decomposed as follows :

$$\begin{aligned}\bar{t}_n&=\begin{Bmatrix}\bar{\tau}_{rz,n}(r)\\ \bar{\sigma}_{zz,n}(r)\\ \bar{\tau}_{\theta z,n}(r)\end{Bmatrix}=\begin{Bmatrix}1\\0\\-1\end{Bmatrix}\frac{\bar{\tau}_{rz,n}(r)-\bar{\tau}_{\theta z,n}(r)}{2}\\&+\begin{Bmatrix}0\\1\\0\end{Bmatrix}\bar{\sigma}_{zz,n}(r)+\begin{Bmatrix}1\\0\\1\end{Bmatrix}\frac{\bar{\tau}_{rz,n}(r)+\bar{\tau}_{\theta z,n}(r)}{2}\\&=\int_0^\infty\begin{Bmatrix}1\\0\\-1\end{Bmatrix}kJ_{n+1}(kr)C_{n+1}(k)dk\\&+\int_0^\infty\begin{Bmatrix}0\\1\\0\end{Bmatrix}kJ_n(kr)C_n(k)dk\\&+\int_0^\infty\begin{Bmatrix}1\\0\\1\end{Bmatrix}kJ_{n-1}(kr)C_{n-1}(k)dk\cdots\cdots(4)\end{aligned}$$

where

$$C_{n+1}(k)=\int_0^{a_0}r\frac{\bar{\tau}_{rz,n}(r)-\bar{\tau}_{\theta z,n}(r)}{2}J_{n+1}(kr)dr,\quad\cdots\cdots(4a)$$

$$C_n(k)=\int_0^{a_0}r\bar{\sigma}_{zz,n}(r)J_n(kr)dr\cdots\cdots(4b)$$

and

$$C_{n-1}(k)=\int_0^{a_0}r\frac{\bar{\tau}_{rz,n}(r)+\bar{\tau}_{\theta z,n}(r)}{2}J_{n-1}(kr)dr\quad\cdots\cdots(4c)$$

The integrals on the right hand sides of Eqs. (4) and (4a)-(4c) are Hankel transform pairs.

The vectors $(1, 0, -1)^T$, $(0, 1, 0)^T$ and $(1, 0, 1)^T$ are the orthogonal eigenvectors corresponding to the eigenvalues $-kJ_{n+1}(kr)$, $kJ_n(kr)$ and $kJ_{n-1}(kr)$ of matrix $\boldsymbol{J}_n$ defined in the following equation.

$$\boldsymbol{J}_n=\begin{bmatrix}J'_n(kr) & 0 & \frac{n}{r}J_n(kr)\\ 0 & kJ_n(kr) & 0\\ \frac{n}{r}J_n(kr) & 0 & J'_n(kr)\end{bmatrix}\cdots\cdots(5)$$

where $J'_n(kr)=\dfrac{dJ_n(kr)}{dr}$. Eq. (4) can then be rewritten as

$$\begin{aligned}\bar{t}_n&=\int_0^\infty-\boldsymbol{J}_n\begin{Bmatrix}1\\0\\-1\end{Bmatrix}C_{n+1}(k)dk\\&+\int_0^\infty\boldsymbol{J}_n\begin{Bmatrix}0\\1\\0\end{Bmatrix}C_n(k)dk\\&+\int_0^\infty\boldsymbol{J}_n\begin{Bmatrix}1\\0\\1\end{Bmatrix}C_{n-1}(k)dk\cdots\cdots(6)\end{aligned}$$

or

$$\bar{t}_n=-\int_0^\infty\boldsymbol{J}_n\boldsymbol{C}_ndk$$

Analytical solution for wave equations in certain layer of **Fig. 1** can be obtained using the technique developed by Sezawa[11]. Using Sezawa's solution, Ref. 2) reported a procedure to obtain the solution for the layered medium shown in **Fig. 1** with the prescribed boundary traction of Eq. (6). By noting the outward normal of the surface of the layered medium is in negative z-direction, the solution of n^{th} Fourier component satisfying the boundary condition of Eq. (6) can be written as

$$\boldsymbol{u}_n=\int_0^\infty\boldsymbol{J}_n\boldsymbol{Q}\boldsymbol{C}_ndk\cdots\cdots(7)$$

In the equation, one should notice that $\boldsymbol{u}_n$ is the displacement vector, at surface $z=0$ in **Fig. 1**, due to the n^{th} Fourier component $\bar{t}_n$ in Eq. (6), and the transfer matrix $\boldsymbol{Q}$ can be found in Ref. 2).

Also, after some mathematical manipulations of making use of Eqs. (4a)-(4c), the identities of $\dfrac{dJ_n(x)}{dx}=\dfrac{J_{n-1}(x)-J_{n+1}(x)}{2}$ and $\dfrac{n}{x}J_n(x)=\dfrac{J_{n+1}(x)-J_{n-1}(x)}{2}$, and Eqs. (3), the vector $\boldsymbol{C}_n$ can be written as

$$\begin{aligned}\boldsymbol{C}_n&=\int_0^{a_0}-\frac{r}{k}\boldsymbol{J}_n\bar{t}_ndr=\int_0^{a_0}-\frac{r}{k}\boldsymbol{J}_n\int_0^{2\pi}\\&\boldsymbol{T}_n\boldsymbol{T}\boldsymbol{H}d\theta drP\frac{1}{a_n}=\boldsymbol{D}_n\boldsymbol{P}\frac{1}{a_n}\cdots\cdots(8)\end{aligned}$$

The complete solution for the prescribed tractions of Eq. (2) can be deduced by simply superposing all the solutions for $n=0, 1, \ldots, \infty$ of both symmetric and anti-symmetric components.

$$\boldsymbol{u}=\sum_{n=0}^{\infty}(\boldsymbol{T}_n^s\boldsymbol{u}_n^s+\boldsymbol{T}_n^a\boldsymbol{u}_n^a)=\sum_{n=0}^{\infty}\left(\left(\boldsymbol{T}_n^s\int_0^{\infty}\boldsymbol{J}_n\boldsymbol{Q}\boldsymbol{D}_n^s dk+\boldsymbol{T}_n^a\int_0^{\infty}\boldsymbol{J}_n\boldsymbol{Q}\boldsymbol{D}_n^a dk\right)\boldsymbol{P}\frac{1}{a_n}\right)\cdots\cdots(9)$$

In the equation, $\boldsymbol{u}_n^s$ and $\boldsymbol{u}_n^a$ are the corresponding solutions for $\bar{t}_n^s$ and $\bar{t}_n^a$ respectively.

To form impedance matrix using Eq. (9), substructuring concept is employed. Consider the layered medium with the prescribed tractions of Eq. (2), the variational principle gives the virtual work of the system :

$$\delta W=\int_0^{a_0}\int_0^{2\pi}\delta\bar{t}_c^T\boldsymbol{u}r d\theta dr\cdots\cdots(10)$$

where $\boldsymbol{u}$ is shown by Eq. (9). Making use of Eqs. (2) and (3), the orthogonal property of Fourier components and the definition of $\boldsymbol{D}_n$ in Eq. (8), Eq. (10) becomes

$$\delta W=\delta\boldsymbol{P}^T\int_0^{\infty}\sum_{n=0}^{\infty}\frac{1}{a_n}\left(\int_0^{a_0}\int_0^{2\pi}\boldsymbol{H}^T\boldsymbol{T}^T\boldsymbol{T}_n^s d\theta\boldsymbol{J}_n r dr\boldsymbol{Q}\boldsymbol{D}_n^s+\int_0^{a_0}\int_0^{2\pi}\boldsymbol{H}^T\boldsymbol{T}^T\boldsymbol{T}_n^a d\theta\boldsymbol{J}_n r dr\boldsymbol{Q}\boldsymbol{D}_n^a\right)dk\boldsymbol{P}$$
$$=-\delta\bar{\boldsymbol{P}}^T\int_0^{\infty}\sum_{n=0}^{\infty}\frac{1}{a_n}(\boldsymbol{D}_n^{sT}\boldsymbol{Q}\boldsymbol{D}_n^s+\boldsymbol{D}_n^{aT}\boldsymbol{Q}\boldsymbol{D}_n^a)k dk\boldsymbol{P}=\delta\boldsymbol{P}^T\boldsymbol{K}\boldsymbol{P}\cdots\cdots(11)$$

Matrix $\boldsymbol{Q}$ of Eq. (7), as reported in Ref. 2), is symmetric, as is the matrix $\boldsymbol{K}$ in Eq. (11).

For the foundation itself, finite elment method in rectangular coordinates is used. After assembling all the elements, the displacement field of the foundation can be written in the form as follows :

$$\bar{\boldsymbol{u}}(x,y)=\boldsymbol{N}(x,y)\boldsymbol{v}\cdots\cdots(12)$$

where matrix $\boldsymbol{N}$ is the assembly of the shape functions assumed in finite elment method, and $\boldsymbol{v}$ is the nodal displacement vector of the foundation finite elment model. Applying the variational principle and making use of Eqs. (1) and (12), the virtual work done is

$$\delta W=\int\int_s\delta\bar{t}^T\bar{\boldsymbol{u}}dA=\delta\bar{\boldsymbol{P}}^T\int\int_s\boldsymbol{H}^T\boldsymbol{N}dA\boldsymbol{v}=\delta\boldsymbol{P}^T\boldsymbol{B}\boldsymbol{v}\cdots\cdots(13)$$

where S denotes the area of the arbitary shape of the foundation, and traction vector $\bar{t}$ and matrix $\boldsymbol{H}$ are defined in Eq. (1).

By observing $\bar{t}$ of Eq. (1) and $\bar{t}_c$ of Eq. (2), one concludes that $\bar{t}$ and $\bar{t}_c$ are the same tractions except described in different coordinate systems. Equating Eq. (13) to Eq. (11) and cancelling out $\delta\boldsymbol{P}^T$, the following equations are obtained.

$$\boldsymbol{K}\boldsymbol{P}=\boldsymbol{B}\boldsymbol{v}\quad\text{or}\quad\boldsymbol{V}=\boldsymbol{B}\boldsymbol{v}\cdots\cdots(14)$$

where vector $\boldsymbol{V}$ is the generalized displacement at the subregions of the assumed piecewise constant traction model. Eq. (14) gives the relationship between the generalized displacement of the traction model of Eq. (1) and the nodal displacement of the finite element model of the foundation. The reciprocal theorem can be employed to obtain the corresponding force-stress relationship for both model : i.e.

$$\boldsymbol{F}=\boldsymbol{B}^T\boldsymbol{P}\cdots\cdots(15)$$

where vector $\boldsymbol{F}$ is the generalized nodal force of the foundation finite element model. Substituting $\boldsymbol{P}=\boldsymbol{K}^{-1}\boldsymbol{B}\boldsymbol{v}$ from Eq. (14) into Eq. (15) yields

$$\boldsymbol{F}=\boldsymbol{B}^T\boldsymbol{K}^{-1}\boldsymbol{B}\boldsymbol{v}=\boldsymbol{I}\boldsymbol{v}\cdots\cdots(16)$$

The matrix $\boldsymbol{I}$ is the impedance matrix for the finite element model of the foundation. Matrix $\boldsymbol{K}$ of Eq. (11) is symmetric, as is the impedance matrix $\boldsymbol{I}$. The interaction stresses can also be calculated using Eq. (14); i.e. $\boldsymbol{P}=\boldsymbol{K}^{-1}\boldsymbol{B}\boldsymbol{v}$.

By examining the numerical scheme of the presented procedure, one will find that most computation effort is devoted to generating matrices $\boldsymbol{D}'_n s$ in Eq. (11) or Eq. (8), which can be obtained using closed form formula with respect to variable θ and Guassian quadrature with respect to variable r. However, the integration of generating $\boldsymbol{D}'_n s$., in which the wave number k is the integration point for the semi-infinite integral in Eq. (11), is independent of excitation frequency ω. In other words, one can generate several impedance matrices for different several frequency components at the same time, if one reserves the storage space in computer for the corresponding matrices $\boldsymbol{K}'s$ in Eq. (11). This feature of the presented procedure will slash the computational cost of generating the impedance matrix for soil-structure interaction analysis.

3. NUMERICAL ANALYSIS

The accuracy of impedance matrix using the presented procedure is dependent upon the following factors :

(1) The numerical integration schemes of using Guassian quadrature,

(2) The truncation of semi-infinite integration limit for the integral in Eq. (11),

(3) The truncation of higher Fourier components in the integrand of Eq. (11),

(4) The subregion size of piecewise constant stress distribution model in Eq. (1).

Among these factors, (1) and (2) have been discussed in details in Reference 2. Therefore, a numerical scheme is designed to investigate the effects of factors (3) and (4).

A soil profile with rigid square foundation is shown in **Fig. 2**, in which different combinations of

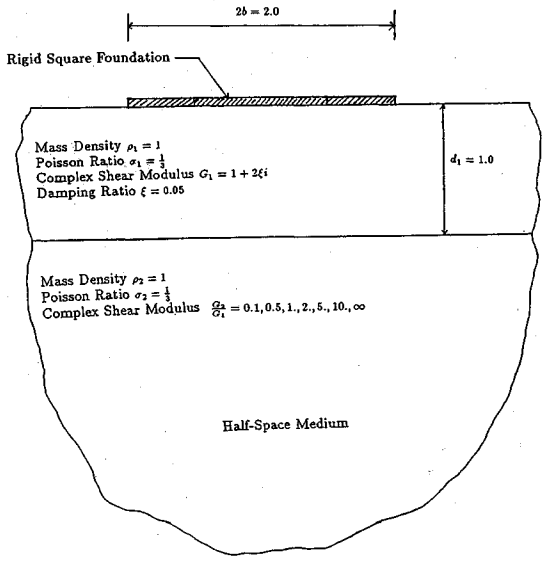

Fig.2 Two-Layer System

soil properties for the two-layer medium are used. The dimensions of the square foundation are assumed to be 2×2 (width $\times$ length). Since all numerical results discussed in the paper will be nondimensionalized, the properties and dimensions in **Fig. 2** are given without units. Employing the symmetric and anti-symmetric properties of the two-layer system, only a quarter model is needed in the studies.

In the study of the effects of neglecting the higher Fourier components and changing the size of subregions (Factors (3) and (4)), the combination of soil properties of the two-layer medium is selected to be $\frac{G_2}{G_1}=2$. **Tables 1~15** show some results of the study. The numerical results in the tables are for the nondimensional frequency $\frac{\omega b}{Re(c_s)}=5.0$, in which c_s is the complex shear wave velocity for the top layer and b is the half-width of the rigid square foundation. Although only the results for $\frac{\omega b}{Re(c_s)}=5$ are presented, the following discussion regarding this study is pertinent for the frequency range with $\frac{\omega b}{Re(c_s)}=0-10$. Also, the results of the impedances have been nondimensionalized with respect to b and G_1 as shown in the tables.

First, the quarter contact area is divided into $m_0\times m_0$ subregions with identical size (see Eq. (1)) in order to check the convergence performance of using identical subregions. The results of $m_0=4$, 7, 10 for torsional, vertical, rocking, coupling and horizontal impedances for the rigid square foundation are shown in **Tables 1~5** respectively. In the tables, nf is the highest Fourier component included in the calculation. From these tables, one can conclude that the impedances are converging as the number of identical subregions increases. Also, one can observe that the numbers for impedances would not change for $nf\geq50$. This means that, up to $m_0=10$ with identical subregion, $nf=50$ is enough in terms of accuracy. However, using

Table 1 Nondimensionalized Torsional Impedance $\left(\frac{K_{TT}}{G_1b^3}\right)$ by Identical Subregions

	4×4	7×7	10×10
nf=50	5.51+11.2 i	5.88+11.4 i	6.05+11.6 i
nf=70	5.51+11.1 i	5.88+11.4 i	6.05+11.6 i
nf=90	5.51+11.1 i	5.87+11.4 i	6.04+11.6 i

Table 2 Nondimensionalized Vertical Impedance $\left(\frac{K_{VV}}{G_1b}\right)$ by Identical Subregions

	4×4	7×7	10×10
nf=50	5.50+40.5 i	5.99+41.0 i	6.18+41.0 i
nf=70	5.51+40.5 i	5.99+41.0 i	6.18+41.0 i
nf=90	5.51+40.5 i	5.99+40.9 i	6.18+41.0 i

Table 3 Nondimensionalized Rocking Impedance $\left(\frac{K_{RR}}{G_1b^3}\right)$ by Identical Subregions

	4×4	7×7	10×10
nf=50	3.23+13.0 i	3.80+13.4 i	4.01+13.6 i
nf=70	3.23+13.0 i	3.80+13.4 i	4.01+13.6 i
nf=90	3.23+13.0 i	3.80+13.4 i	4.00+13.6 i

Table 4 Nondimensionalized coupling Impedance $\left(\frac{K_{HR}}{G_1b^2}\right)$ by Identical Subregions

	4×4	7×7	10×10
nf=50	0.050−0.880 i	0.315−0.915 i	0.375−0.917 i
nf=70	0.049−0.880 i	0.309−0.915 i	0.371−0.917 i
nf=90	0.048−0.880 i	0.308−0.915 i	0.370−0.917 i

Table 5 Nondimensionalized Horizontal Impedance $\left(\frac{K_{HH}}{G_1b}\right)$ by Identical Subregions

	4×4	7×7	10×10
nf=50	4.82+17.8 i	4.97+18.0 i	5.06+18.1 i
nf=70	4.82+17.8 i	4.97+18.0 i	5.06+18.1 i
nf=90	4.82+17.8 i	4.97+18.0 i	5.06+18.1 i

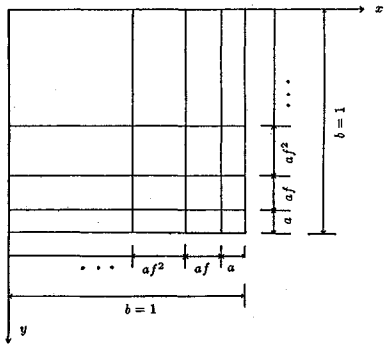

Fig.3 Meshing Scheme with Sequential Enlargement of Subregions

identical subregions the convergence performance seems not good enough in terms of computational cost. The reason for this situation is the interaction stresses vary sharply at the edges of the contact area. This will be confirmed by the distributions of the interaction stresses shown later. Therefore, using smaller subregions at the edges of contact area is advised.

A meshing scheme is devised to address the problem of rapid change of interaction stresses at edges of contact area. **Fig. 3** shows the scheme of varied size of subregions. In the scheme, the subregion at the corner of the quarter contact area is smallest, and the spacing of dividing lines for subregions is enlarged in sequence by a factor f for both edges of the quarter contact area as shown in **Fig. 3**. Now, the quarter contact area is divided into 10×10 subregions (100 in total), and $f=1.15$ and 1.23 are selected, which are equivalent to 20×20 and 30×30 identical subregions respectively for the subregion at the corner of the quarter contact area. The results together with that of using 10×10 identical subregions ($f=1.00$) are shown in **Tables 6~10**. By examining these 5 tables, the following three conclusions can be drawn :

(1) The difference between the numerical results for $f=1.15$ and $f=1.23$ in the tables is small. Therefore, if the meshing scheme is equivalent to 20×20 identical subregions or more, good results can be obtained.

(2) Using varied subregions gives better results than using identical subregions in terms of computational cost.

(3) By observing the numerical results for $f=1.00$ and $f=1.15$ in the tables, one can find that $nf=50$ is enough for $f=1.00$ and $nf=70$ is needed for $f=1.15$ if good accuracy is wanted for both meshing schemes. Therefore, the smaller the subregion at the corner is, the more the Fourier components with respect to θ in Eq. (11) is needed in order to obtain good accuracy.

Table 6 Nondimensionalized Torsional Impedance $\left(\frac{K_{TT}}{G_1b^3}\right)$ by Varied Subregions

	10×10, f=1.0	10×10, f=1.15	10×10, f=1.23
nf=50	6.05+11.6*i*	6.25+12.1*i*	6.33+12.2*i*
nf=70	6.05+11.6*i*	6.21+12.0*i*	6.26+12.1*i*
nf=90	6.04+11.6*i*	6.20+12.0*i*	6.24+12.1*i*
nf=110		6.20+12.0*i*	6.23+12.0*i*

Table 7 Nondimensionalized Vertical Impedance $\left(\frac{K_{VV}}{G_1b}\right)$ by Varied Subregions

	10×10, f=1.00	10×10, f=1.15	10×10, f=1.23
nf=50	6.18+41.0*i*	6.33+42.0*i*	6.34+42.1*i*
nf=70	6.18+41.0*i*	6.32+41.9*i*	6.33+42.0*i*
nf=90	6.18+41.0*i*	6.32+41.9*i*	6.32+41.9*i*
nf=110		6.32+41.9*i*	6.32+41.9*i*

Table 8 Nondimensionalized Rocking Impedance $\left(\frac{K_{RR}}{G_1b^3}\right)$ by Varied Subregions

	10×10, =1.00	10×10, f=1.15	10×10, f=1.23
nf=50	4.01+13.6*i*	4.25+14.2*i*	4.33+14.3*i*
nf=70	4.01+13.6*i*	4.23+14.2*i*	4.26+14.2*i*
nf=90	4.00+13.6*i*	4.22+14.2*i*	4.27+14.2*i*
nf=110		4.22+14.2*i*	4.26+14.2*i*

Table 9 Nondimensionalized coupling Impedance $\left(\frac{K_{HR}}{G_1b^2}\right)$ by Varied Subregions

	10×10, f=1.00	10×10, f=1.15	10×10, f=1.23
nf=50	0.375−0.917*i*	-0.033−0.879*i*	-0.028−0.877*i*
nf=70	0.371−0.917*i*	-0.034−0.879*i*	-0.033−0.880*i*
nf=90	0.370−0.917*i*	-0.035−0.879*i*	-0.033−0.880*i*
nf=110		-0.035−0.879*i*	-0.034−0.880*i*

Table 10 Nondimensionalized Horizontal Impedance $\left(\frac{K_{HH}}{G_1b}\right)$ by Varied Subregions

	10×10, f=1.00	10×10, f=1.15	10×10, f=1.23
nf=50	5.06+18.1*i*	5.14+18.6*i*	5.15+18.6*i*
nf=70	5.06+18.1*i*	5.13+18.5*i*	5.13+18.6*i*
nf=90	5.06+18.1*i*	5.13+18.5*i*	5.13+18.5*i*
nf=110		5.13+18.5*i*	5.12+18.5*i*

Therefore, the scheme of sequentially varied subregions is suggested in the investigation that follows.

In order to save some computational cost, smaller number of subregions for contact area is desired. Comparisons of the results with different

Table 11 Nondimensionalized Torsional Impedance $\left(\frac{K_{TT}}{G_1 b^3}\right)$ by Varied Subregions

	4×4, f=2.57	7×7, f=1.48	10×10, f=1.23
nf=50	6.56+12.1i	6.34+12.1i	6.33+12.2i
nf=70	6.53+12.0i	6.28+12.0i	6.26+12.1i
nf=90	6.51+12.0i	6.25+12.0i	6.24+12.1i
nf=110		6.24+12.0i	6.23+12.0i

Table 12 Nondimensionalized Vertical Impedance $\left(\frac{K_{VV}}{G_1 b}\right)$ by Varied Subregions

	4×4, f=2.57	7×7, f=1.48	10×10, f=1.23
nf=50	6.48+41.6i	6.27+42.0i	6.34+42.1i
nf=70	6.47+41.6i	6.25+41.9i	6.33+42.0i
nf=90	6.46+41.6i	6.25+41.8i	6.32+41.9i
nf=110		6.24+41.8i	6.32+41.9i

Table 13 Nondimensionalized Rocking Impedance $\left(\frac{K_{RR}}{G_1 b^3}\right)$ by Varied Subregions

	4×4, f=2.57	7×7, f=1.48	10×10, f=1.23
nf=50	5.03+14.4i	4.36+14.3i	4.35+14.3i
nf=70	4.99+14.3i	4.32+14.2i	4.28+14.2i
nf=90	4.98+14.3i	4.30+14.2i	4.27+14.2i
nf=110		4.29+14.2i	4.26+14.2i

Table 14 Nondimensionalized coupling Impedance $\left(\frac{K_{HR}}{G_1 b^2}\right)$ by Varied Subregions

	4×4, f=2.57	7×7, f=1.48	10×10, f=1.23
nf=50	-0.074−0.820i	-0.029−0.871i	-0.028−0.877i
nf=70	-0.077−0.820i	-0.032−0.872i	-0.033−0.880i
nf=90	-0.078−0.820i	-0.033−0.872i	-0.033−0.880i
nf=110		-0.033−0.872i	-0.034−0.880i

Table 15 Nondimensionalized Horizontal Impedance $\left(\frac{K_{HH}}{G_1 b}\right)$ by Varied Subregions

	4×4, f=2.57	7×7, f=1.48	10×10, f=1.23
nf=50	5.14+18.6i	5.11+18.5i	5.15+18.6i
nf=70	5.13+18.6i	5.09+18.5i	5.13+18.6i
nf=90	5.12+18.6i	5.08+18.5i	5.13+18.5i
nf=110	5.12+18.6i	5.08+18.5i	5.12+18.5i

numbers of subregions and amplification factors are made in **Tables 11~15**. In the tables, all the meshing schemes (4×4 and f=2.67, 7×7 and f=1.48, 10×10 and f=1.23) are equivalent to 30×30 identical subregion meshing scheme for the subregion at the corner of the quarter contact area. From

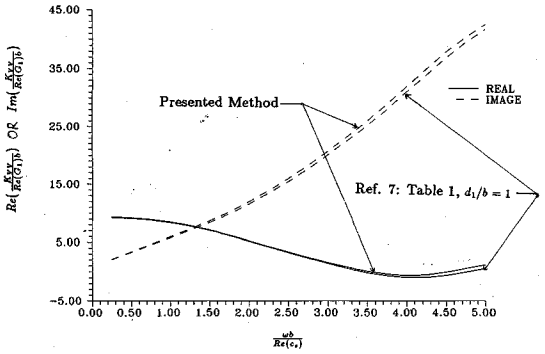

Fig.4 Comparison of Nondimensionalized Vertical Impedance

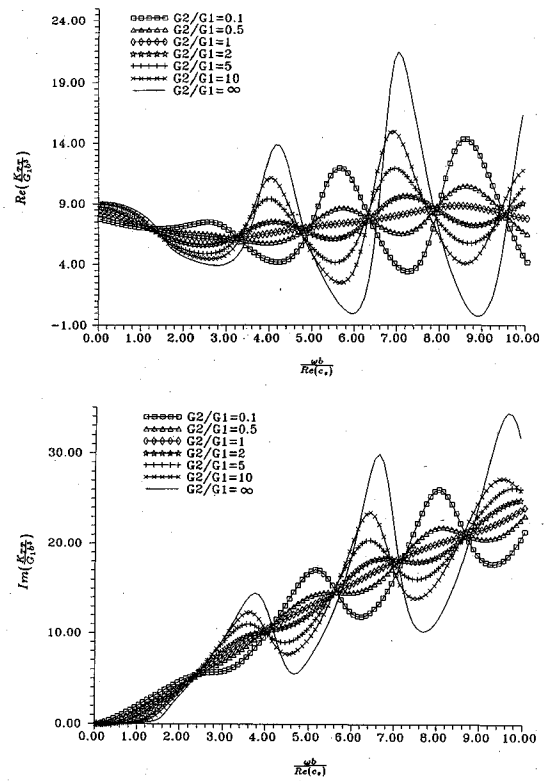

Figs.5 a and b Nondimensionalized Torsional Impedance

these tables and **Tables 1~5**, one can observe that the impedances do converge as the number of subregions and the number of included Fourier components increase. Also, as compared with the corresponding table of **Tables 1~5**, one can conclude that using varied meshing scheme for the contact area can result in higher accuracy and lower computational cost. Therefore, the varied meshing scheme is suggested for contact area of rigid foundation and surrounding soil.

For demonstrating the effectiveness of the

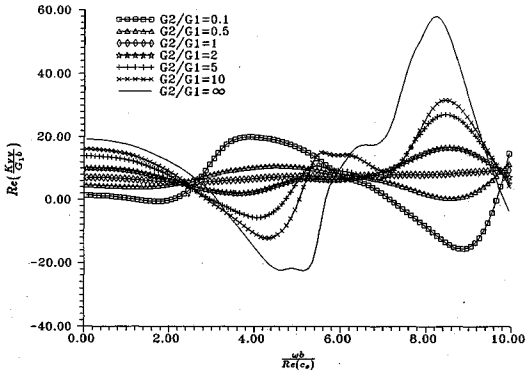

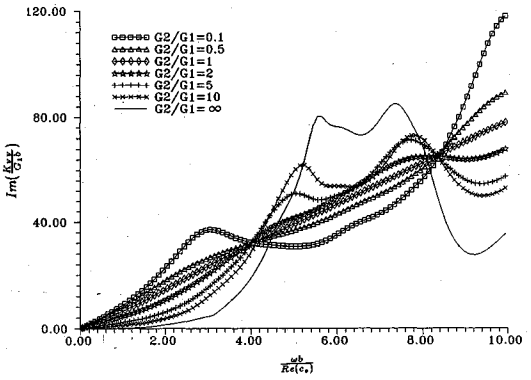

Figs.6 a and b Nondimensionalized Vertical Impedance

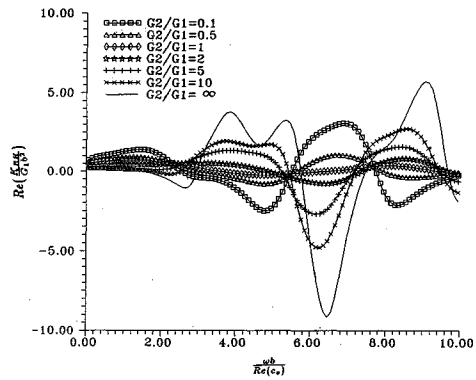

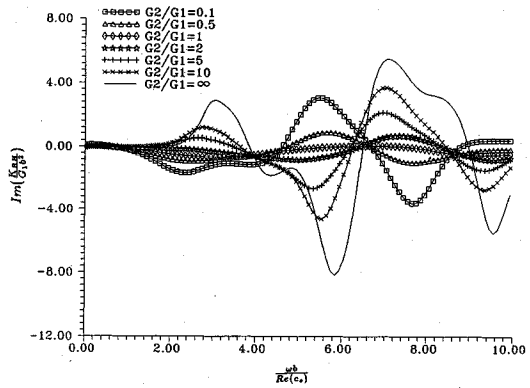

Figs.8 a and b Nondimensionalized Coupling Impedance

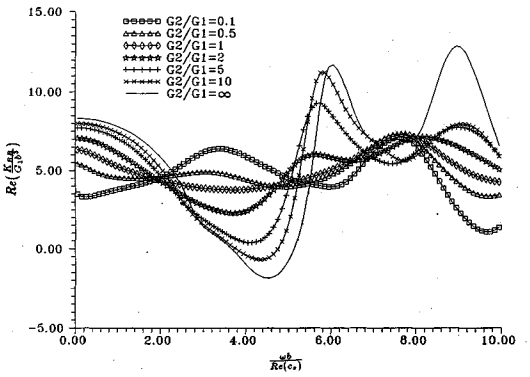

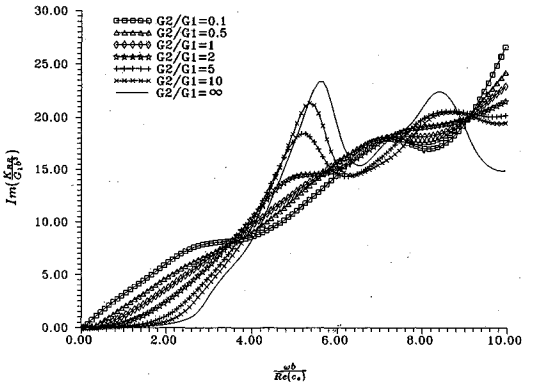

Figs.7 a and b Nondimensionalized Rocking Impedance

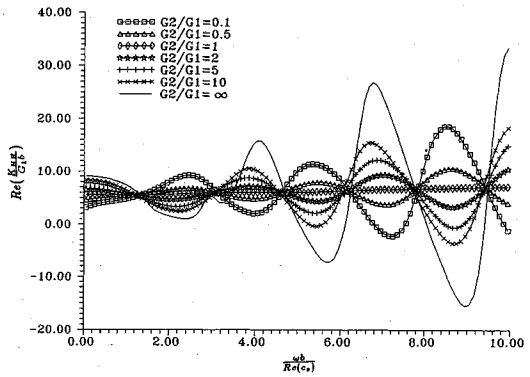

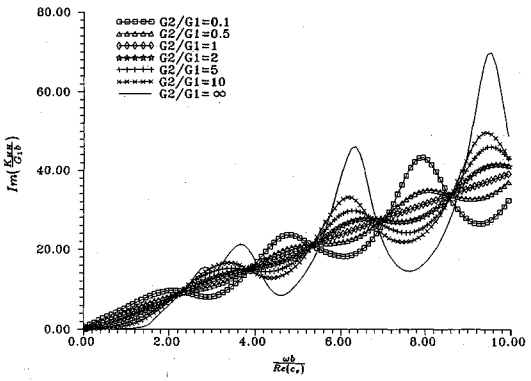

Figs.9 a and b Nondimensionalized Horizontal Impedance

presented procedure, a comparison with previous work (Ref. 7) is made in **Figs. 4** for the vertical vibration of a rigid square foundation on a two-layer medium. The meshing scheme of quarter contact area is 4×4 with amplification factor $f=2.50$, and the highest Fourier component included in the calculation is 50 ($nf=50$) for the presented method. From the figure, one can observe that both results match each other pretty well.

An example of the two-layer system shown in **Fig. 2** is employed to investigate the effect of layered stratum on impedance matrices. In the example, the meshing scheme of the quarter area is also 4×4 with amplification factor $f=2.50$, and the highest Fourier component included in the calculation is also 50 ($nf=50$). According to **Tables 11～15** and some other investigation, the impedances for torsional, vertical, rocking and horizontal vibrations of the foundation is believed to be less than 2% inaccurate and the inaccuracy for coupling impedance is somewhat higher (about 6% in Table 14). **Figs. 5～9** show the torsional, vertical, rocking, coupling and horizontal impedance functions respectively. One also should notice that all the impedances and frequency in the figures are nondimensionalized.

From **Figs. 5a, 6a, 7a** and **9a**, one can observe that the real parts of the impedances for the layered system fluctuate along the curves of the real parts of the corresponding impedances for the half-space medium $\left(\frac{G_2}{G_1}=1.0\right)$, and the fluctuations become more dramatic as the lower half-space layer goes stiffer or softer with respect to the top layer. This phenomenon can be explained as the influence of the reflection waves from the horizontal interface of the two-layer system. For softer half-space medium ($G_2<G_1$), the real parts of the impedances (except the coupling impedance) is smaller at lower frequency range. Whereas, the real parts of the impedances is larger for the stiffer half-space medium. This comfirms that the static stiffness for the foundation becomes greater as the lower half-space medium goes stiffer.

The imaginary parts of impedances for torsional, vertical, rocking, and horizontal motions of the square foundation are shown in **Figs. 5b, 6b, 7b, 9b** respectively. From these figures, one can conclude that the radiation damping for stiffer lower half-space medium is smaller in the lower frequency range. This is opposite to the nature of the real parts of the impedances as stated above. **Figs.** 8a and 8b show the coupling impedance for rocking and horizontal motions of the square foundation. These two figures indicate that the coupling impedance in soil-structure interaction

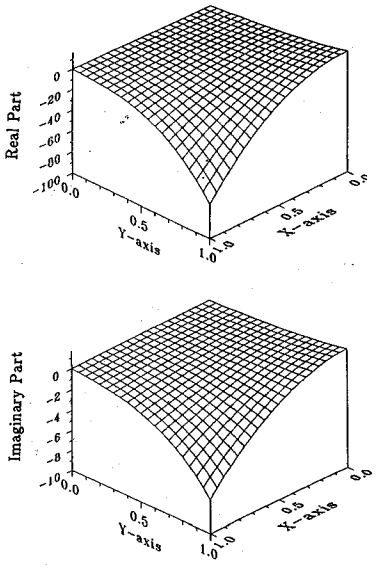

Fig.10 τ_{xz} Component of Interaction Stresses by Torsional Vibration

analysis can not be neglected especially for the case with layered stratum.

According to Eq. (1), the assumed distribution of interaction stresses is piecewise constant on the contact area. Curve fitting with least square method is employed in order to obtain continueous distribution of interaction stresses on X-Y plane (contact area). The curve fitting function is assumed as follows :

$$C(x,y)=f(x)g(y) \quad \cdots\cdots(17)$$

where functions $f(x)$ and $g(y)$ are polynominal functions. After some extensive study, the polynominal functions with order 5 is enough for all the components of interaction stresses : i.e.

$$f(x)=a_5x^5+a_4x^4+a_3x^3+a_2x^2+a_1x+a_0,$$

$$g(y)=b_5y^5+b_4y^4+b_3y^3+b_2y^2+b_1y+b_0,$$

The coefficients $a's$ and $b's$ are determined by least square method.

Figs 10～13 show the typical distributions of interaction stresses for the case of $\frac{G_2}{G_1}=2.0$ and $\frac{\omega b}{Re(c_s)}=0.05$. The stress magnitudes in the figures are obtained by assuming the complex shear modulus $G_1=1+0.1i$ ($\xi=0.05$) and the vibration amplitude of the rigid square foundation $v=1.$ in Eq. (12). For each vibration, only major component of interaction stresses is shown in the figure, since the other two components are either much smaller by one order or similar to the major component. Also, the interaction stresses are plotted only for a quarter of the contact area due to

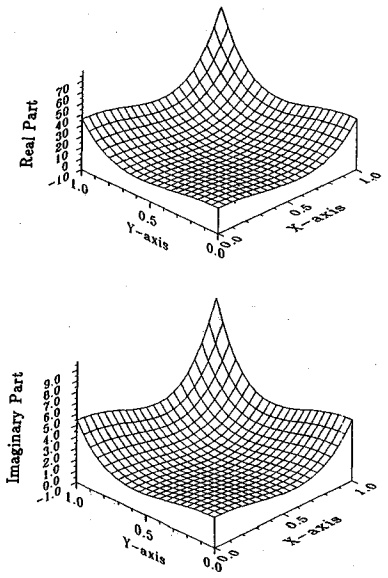

Fig.11 σ_{zz} Component of Interaction Stresses by Vertical Vibration

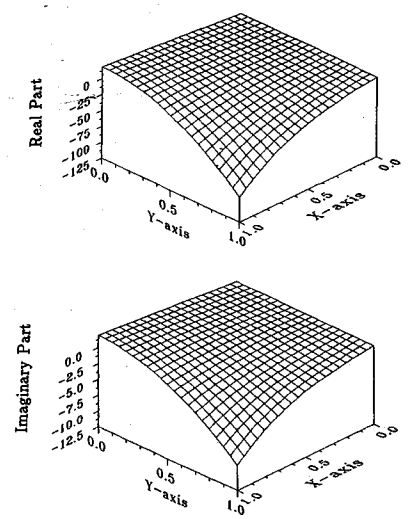

Fig.12 σ_{zz} Component of Interaction Stresses by Rocking Vibration

the nature of symmetry or anti-symmetry with respect to x-axis and y-axis.

From these figures, one can observe that the maximums of the major components of interaction stresses always occur at the corners of contact area, and the major components of interaction stresses rise or drop sharply near the edges of contact area. These phenomenons confirm that the singularity of interaction stresses could occurs at the corner of contact area, and prove that the meshing scheme, as discussed previously with **Fig. 3**, is reasonable.

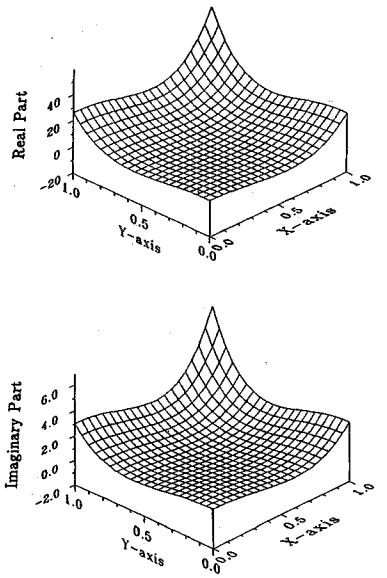

Fig.13 τ_{xz} Component of Interaction Stresses by Horizontal Vibration

4. ACKNOWLEDGEMENTS

This work is sponsored by National Science Council of Taiwan under the contract No. NSC80-0410-E009-19. The numerical computions are performed in SUN IV work station at Department of Civil Engineering, National Chiao-Tung University. These supports are greatly appreciated.

REFERENCES

1) Liou, G.-S. : Analytical Solution for Soil-Structure Interaction in Layered Media, Jour. of Earthquake Engineering and Structural Dynamics, Vol. 18, 667-686, 1989.
2) Liou, G.-S. and Lee, G. C. : Impedance Matrices for Axial Symmetric Foundations on Layered Media, Structural Eng./Earthquake Eng., JSCE, Vol. 9, No. 1, 33-44, 1992.
3) Liou, G.-S. : Vibration of Surface Foundations of Arbitary Shapes, Jour. of Earthquake Engineering and Structural Dynamics, Vol. 20, 1115-1125, 1991.
4) Tzong, T.-J. and Penzien, J. : Hybrid-Modelling of Soil-Structure Interaction in Layered Media, UBC/EERC-83/22, Oct. 1983.
5) Kausel, E. : Forced Vibrations of Circular Foundations on Layered Media, R74-11, Dept. of Civil Eng., MIT, Jan. 1974.
6) Chapel, F. : Boundary Element Method Applied to Linear Soil-Structure Interaction on a Heterogeneous Soil, Jour. of Earthquake Engineering and Structural Dynamics, Vol.15, 815-829, 1987.
7) Wong, H. L. and Luco, J. E. : Tables of Impedance functions for Square Foundations on Layered Media, Jour.

of Soil Dynamics and Earthquake Engineering, Vol.4, 64-81, 1985.

8) Wolf, J. P. and Darbre, G. R. : Dynamic Stiffness Matrix of Soil by Boundary Element Method : Conceptual Aspects, Jour. of Earthquake Engineering and Structural Dynamics, Vol.12, 385-400, 1984.

9) Lysmer, J. : Vertical Motion of Rigid Footings, Contract Report No. 3-115, Dept. of Civil Eng., Univ. of Michigan, 1965.

10) Wong, H. L. and Luco, J. E. : Dynamic Response of Rigid Foundations of Arbitary Shape, Jour. of Earthquake Engineering and Structural Dynamics, Vol.4, 579-587, 1976.

11) Sezawa, K. : Further Studies on Rayleigh Waves Having Some Azimuthal Distribution, Bulletin of Earthquake Research Institute, Tokyo, Vol.6, 1-81, 1929.

(Received May 26, 1992)